Timing of rock-uplift and of the North Anatolian Fault development in the Central Pontides (Turkey)

Racano S.[1-2], Schildgen T.[2], Ballato P.[3]

1 Universität Potsdam, Institut für Geowissenschaften

2 GFZ German Research Centre for Geosciences

3 University of Roma Tre, Department of Science

Geological background

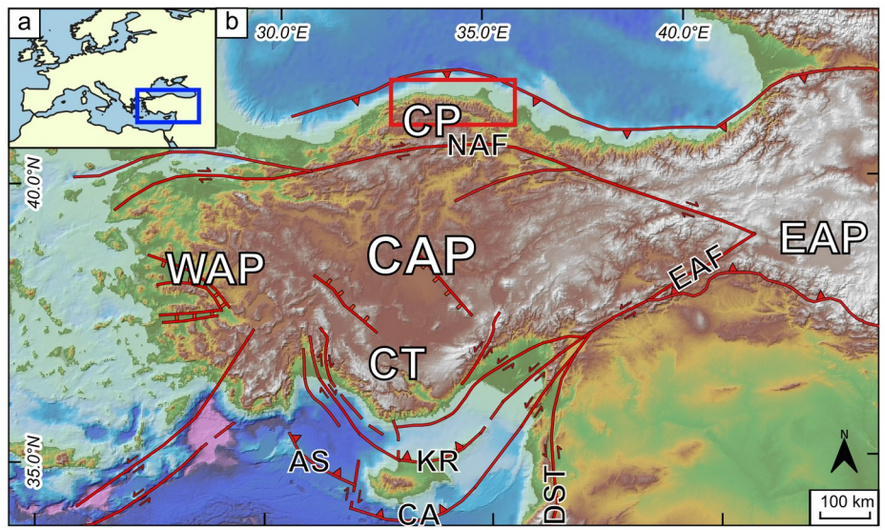

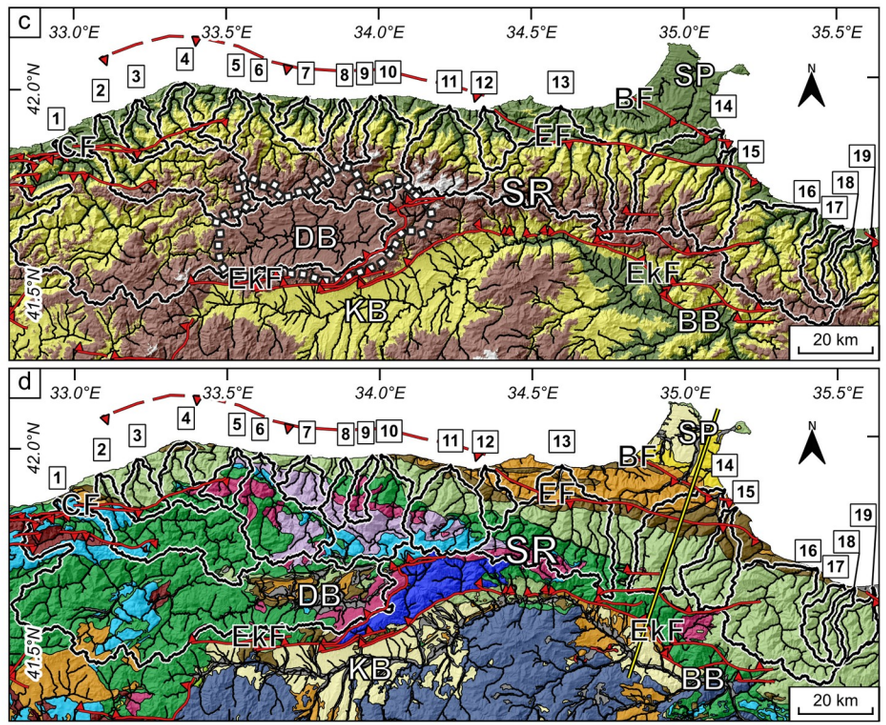

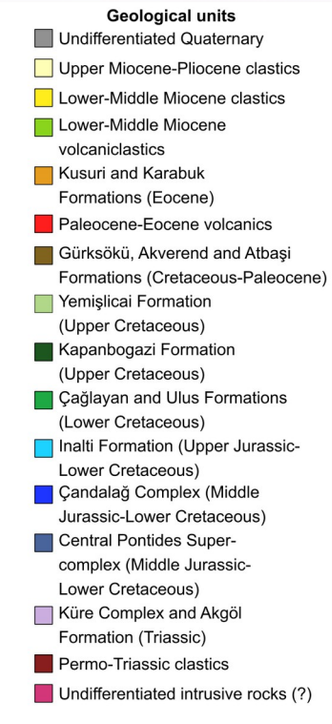

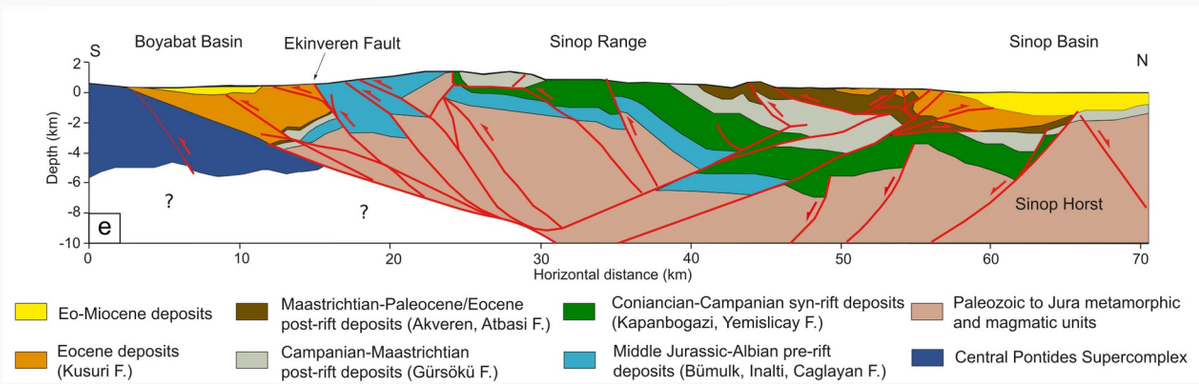

a-b) location of the study area;

c) elevations and main structures of the Sinop Range;

d) geological map of the Sinop Range and trace of the cross section (yellow line);

e) geological cross section.

CAP: Central Anatolian Plateau; **EAP**: Eastern Anatolian Plateau; **WAP**: Western Anatolian Province; **CP**: Central Pontides; **CT**: Central Taurides; **NAF**: North Anatolian Fault; **EAF**: East Anatolian Fault; **DST**: Death Sea Transform Fault; **CA**: Cyprus Arc; **PT**: Paphos Transform; **AS**: Antalya Slab; **SR**: Sinop Range; **SP**: Sinop Peninsula; **DB**: Devrekani Basin; **KB**: Kastamonu Basin; **BB**: Boyabat Basin; **BF**: Balıfakı Fault; **EF**: Erikli Fault; **CF**: Cide Fault; **EkF**: Ekinveren Fault.

Geological background

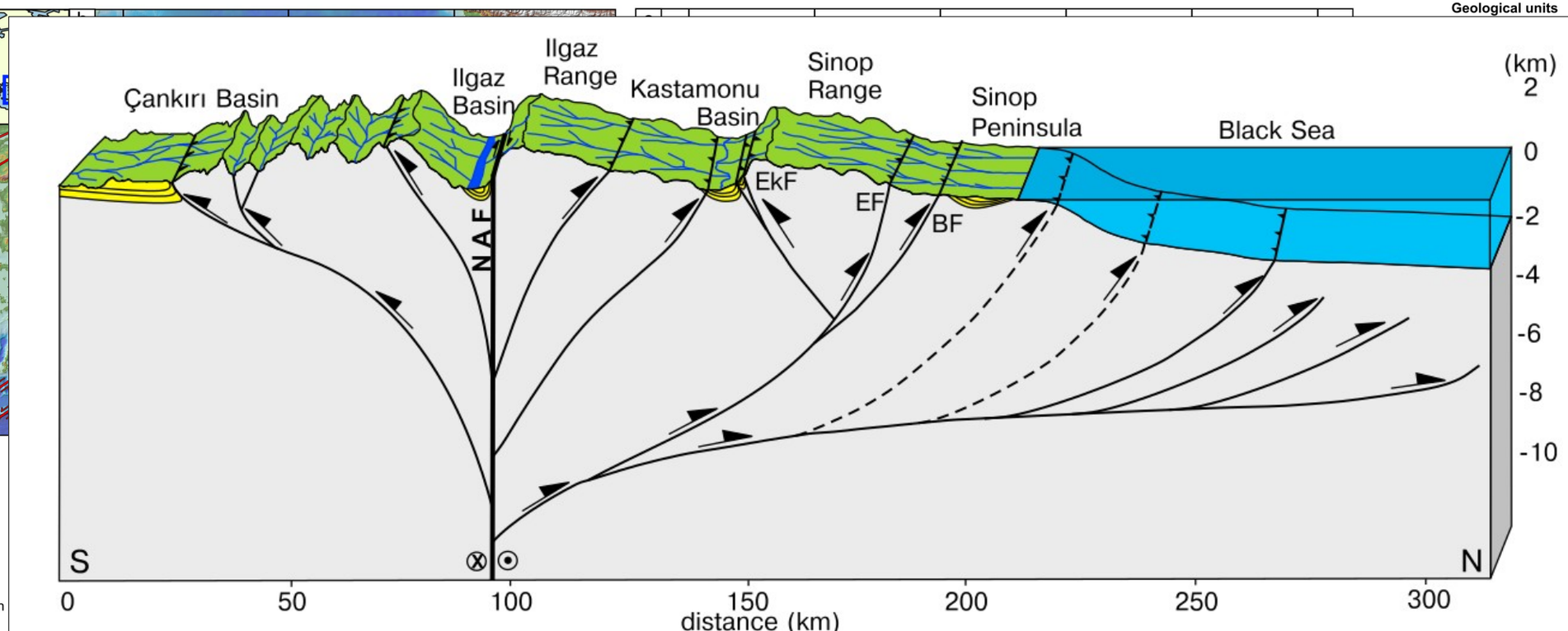

Figure 16. A conceptual model for the Central Pontides, which demonstrate an active orogenic wedge related to positive flower structure developed over a shallow detachment surface linked to North Anatolian Fault at depth. Structures south of the NAF are based on interpretations from *Kaymakçı et al.* [2010]. Yellow areas are schematic representations of deformed Neogene deposits in the Sinop Peninsula and intermontane basins. BF: Balıfakı Fault, EF: Erikli Fault, EkF: Ekinveren Fault, KyF: Kayı Fault, NAF: North Anatolian Fault. Vertical exaggeration = 7.

Yıldırım et al., 2011

ection

WAP:
urides;
th Sea
ntalya
n; **KB**:

Kastamonu Basin; **BB**: Boyabat Basin; **BF**: Balıfakı Fault; **EF**: Erikli Fault; **CF**: Cide Fault; **EkF**: Ekinveren Fault.

Exhumation history (Ballato et al., 2018)

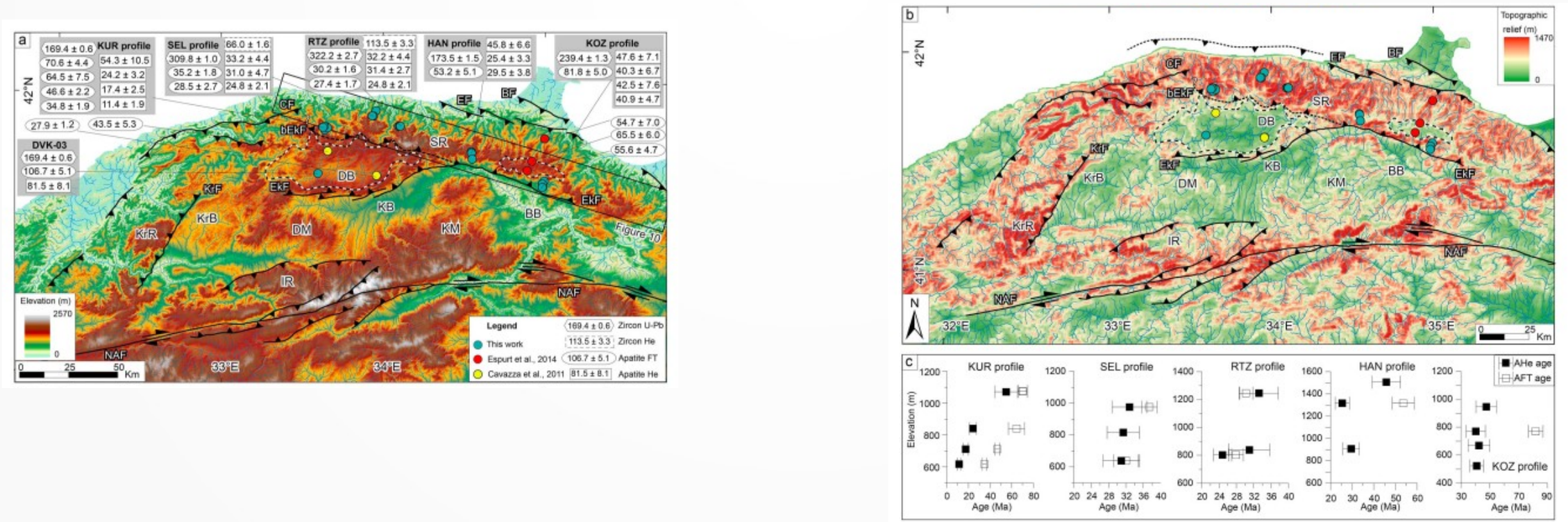

Figure 2. (a) Digital Elevation Model and (b) topographic relief map calculated over a 2-km circular radius superimposed over a hillshade model of the Central Pontides, showing major faults (modified after Yıldırım et al., 2011), Zircon U-Pb, AFT, and AHe ages. BF = Balıfakı Fault; CF = Cide Fault; EF = Erikli Fault; EkF = Ekinveren Fault; bEkF = Blind Ekinveren Fault; KF = Karabük Fault; NAF = North Anatolian Fault; IR = Ilgaz Range; KrR = Karabük Range; SR = Sinop Range; BB = Boyabat Basin; DB = Devrekani Basin; KrB = Karabük Basin; KB = Kastamonu Basin; DM = Daday Massif; KM = Kargı Massif. Note the arc-shaped, elevated, and high-relief topography of the Sinop and Karabük ranges (SR and KrR, respectively). These ranges are bounded by inward dipping reverse faults, extend parallel to the cost and tend to merge with the NAF and associated topography. Moreover, they delimit a semicircular and elevated low relief area that includes metamorphic massifs (DM and KM), Cretaceous to Eocene marine basins (BB, KrB, and DB) and a Mio-Pliocene continental basins (KB). (c) Age versus topographic elevation plots of vertical profile shown in Figure 2a. The dashed lines show the inferred location of a blind thrust fault defined in the text as the bEkF and the offshore continuation of the Erikli Fault.

Exhumation history (Ballato et al., 2018)

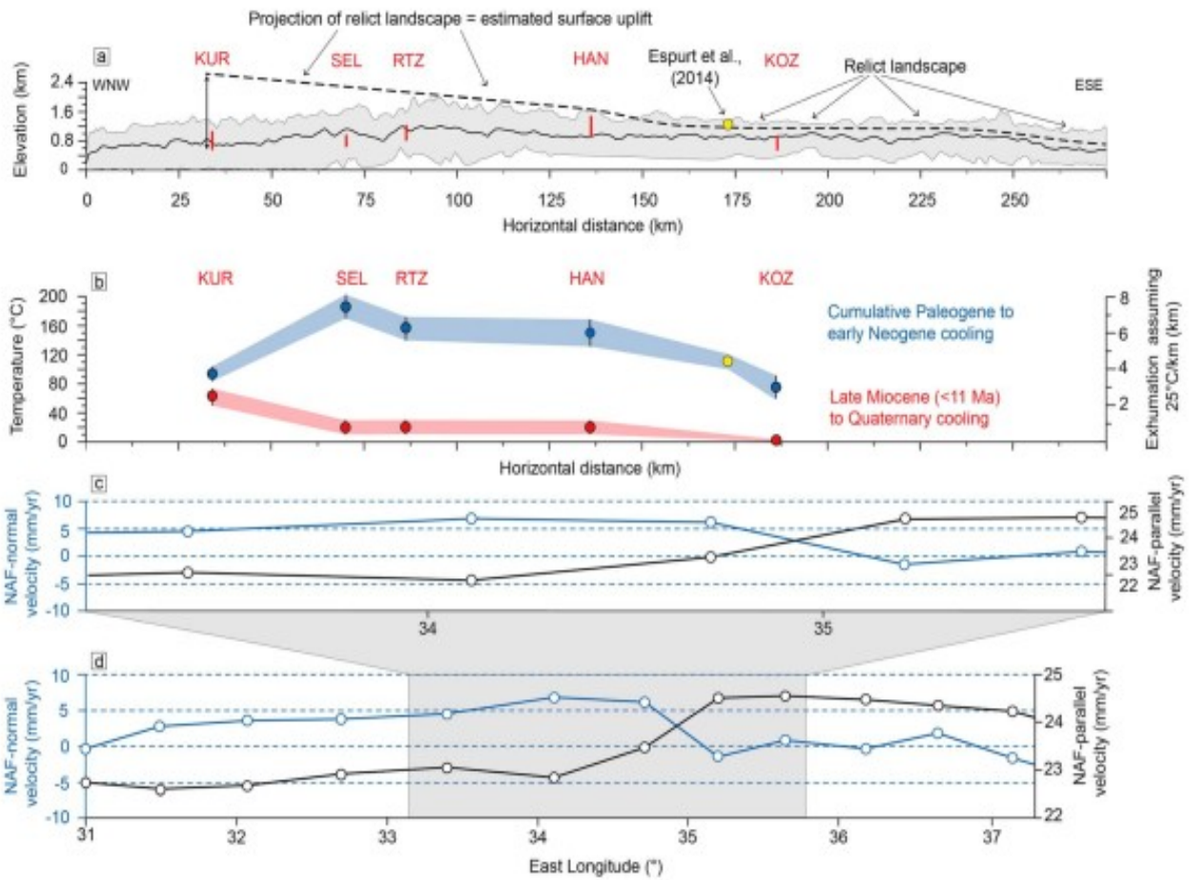

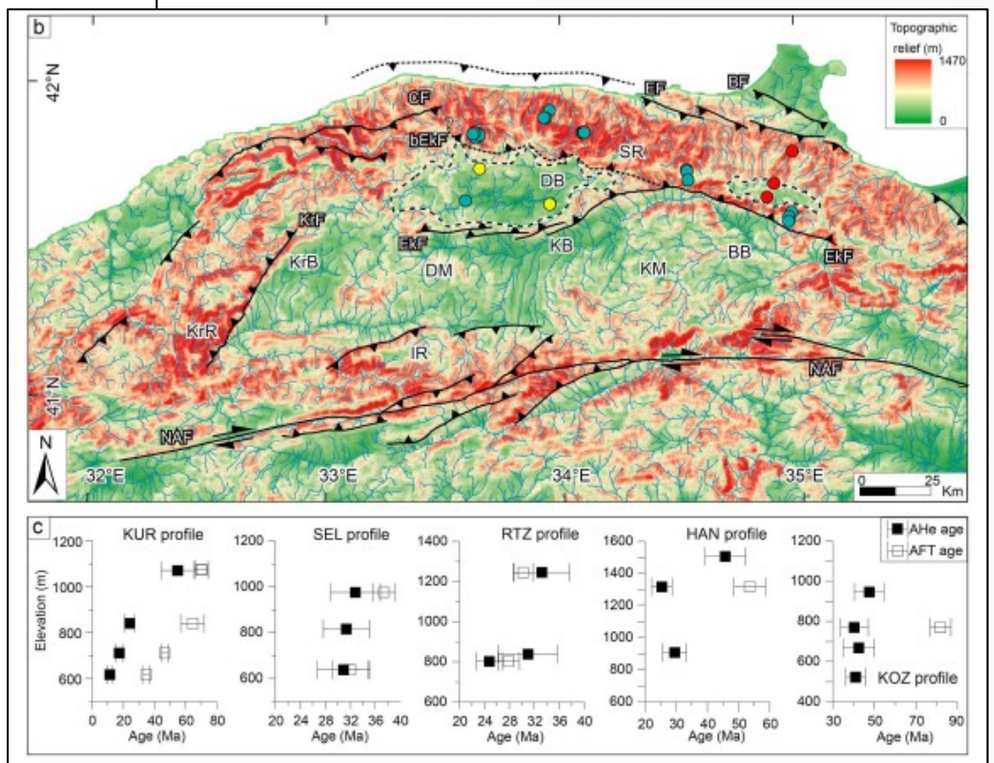

Figure 10. (a) Location of sampled vertical profiles (red thick line) projected over a topographic swath profile (see Figure 2 for location). The black dashed line represents the interpolation and the projection of the relict landscape (see Figure 2) for the eastern and western sectors, respectively (see text for further explanation). (b) Cumulative Paleogene and Late Cenozoic cooling and supposed exhumation. Note that the Paleogene pattern of cooling is characterized by a maximum in the central sectors of the Sinop Range, while in the Late Cenozoic, cooling was focused in the western sectors of the profile, where topographic relief is greater (see Figure 2). (c and d) Close-up (see black thick frame of Figure 10d for location) and regional view of Global Positioning System-derived fault normal (blue) and fault parallel (black) slip rates along the North Anatolian Fault (redrawn from Yıldırım et al., 2011), with positive fault-normal values indicating compression. Note that the Late Cenozoic cooling pattern roughly mimics the fault normal slip component of the North Anatolian Fault (NAF) and the inferred elevation of the relict landscape.

Detachment-limited rivers

(1) $$\frac{dz(t,x)}{dt} = U(t,x) - E(t,x)$$

(2) $$E = K A^m S^n$$

(3) $$S = \left(\frac{E}{K}\right)^{\frac{1}{n}} A^{-\frac{m}{n}}$$

(4) $$\left(\frac{E}{K}\right)^{\frac{1}{n}} = \left(\frac{U}{K}\right)^{\frac{1}{n}} = A^{-\frac{m}{n}} S = k_s$$

For m/n ref. $k_s \longrightarrow k_{sn}$

- z = elevation;
- t = time;
- U = rock-uplift;
- E = erosion;
- A = upstream drainage area;
- S = channel slope;
- K = erosion parameter;
- A = upstream drainage area
- k_s = channel steepness index;
- m & n = positive coefficients related respectively to basin hydrology and erosion processes in the bedrock channel. In linear conditions n=1 and $0.3<m<0.5$;
- k_{sn} = normalized steepness index (k_s for a reference m/n ratio)

Howard & Kerby, 1983; Whipple & Tucker, 1999

Solving equation 1 for block-uplift scenario and n=1

(1) $$\frac{dz(t,x)}{dt} = U(t,x) - E(t,x)$$

(5) $$z(x) = \int_{-\tau(x)}^{0} U(t')\,dt'$$

(6) $$\tau = \int_{x_b}^{x} \frac{dx'}{K(x')A(x')^m}$$

- z = elevation;
- t = time;
- U = rock-uplift (spatially constant, time variable);
- E = erosion;
- A = upstream drainage area;
- K = erosion parameter;
- x_b = stream channel base-level;
- x = arbitrary upstream point;
- τ = travel time of a perturbation along the river profile from the river outlet (x=0) to a given point x;

Whipple & Tucker, 1999; Goren et al., 2014; Gallen., 2018

Non-dimensional uplift history from river χ-plots (Goren et al., 2014)

(7) $$\tau = \int_{x_b}^{x} \frac{dx'}{K(x')A(x')^m} K(x') A_0^m \longrightarrow \chi(x) = \int_{x_b}^{x} \left(\frac{A_0}{A(x')} \right)^m dx'$$

(8) $$z(x) = z(x_b) + \left(\frac{U}{K A_0^m} \right)^{\frac{1}{n}} \chi$$ Equation of the χ-plot (Perron & Royden, 2013)

(9) $$\frac{U}{K A_0^m} = U^*$$ Non-dimensional uplift (slope of the χ-plot)

(10) GU*=z **New form of Eq. 8 used for the inversion. The data organization assumes that N data points of z and χ along the fluvial network are ordered according to elevation because they share a common rock-uplift history.**

(11) $$\mathbf{U^*} = U^*_{pri} + (\mathbf{G}^T\mathbf{G} + \Gamma^2\mathbf{I})^{-1}\mathbf{G}^T(\mathbf{z} - \mathbf{G}U^*_{pri})$$ Least-squares estimate for U* (following Tarantola, 1998)

(12) $$U^*_{pri} = \left(\frac{1}{N} \right) \sum_{i=1}^{N} \left(z_i / \sum_{j=1}^{q} A_{i,j} \right)$$ Average slope of the inverted χ-plot

- A = upstream drainage area;
- A_0 = reference drainage area;
- K = erosion parameter;
- x_b = stream channel base-level;
- x = arbitrary upstream point;
- χ = obtained by removing K from Equation 6, it represents the non-dimensional time
- **U*** = non-dimensional uplift
- **G** = N x q matrix, where N is a set of data points of z and χ along the fluvial network that share a common uplift history and are ordered according to elevation, q is the number of discrete χ steps;
- $z(x_b)$ = baselevel (set=0 in the inversion);
- Γ = dampening coefficient that determines the smoothness imposed on the solution;
- **I** = $q \times q$ identity matrix;
- U^*_{pri} = prior guess at the uplift rate

Fixing U^*_{pri}

Racano et al., 2021

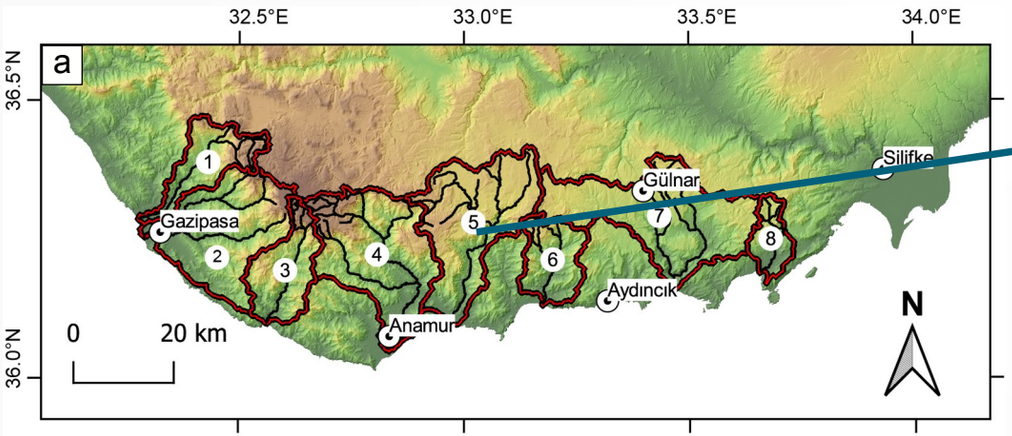

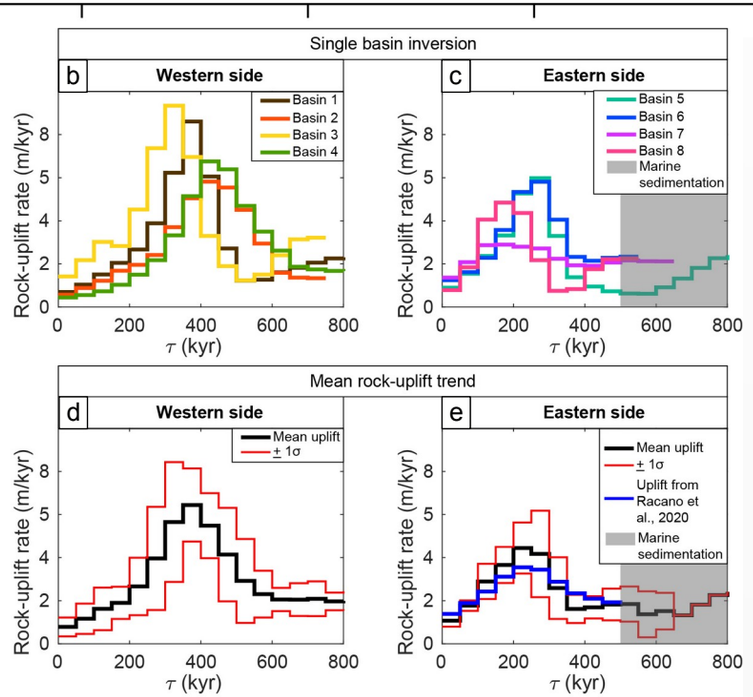

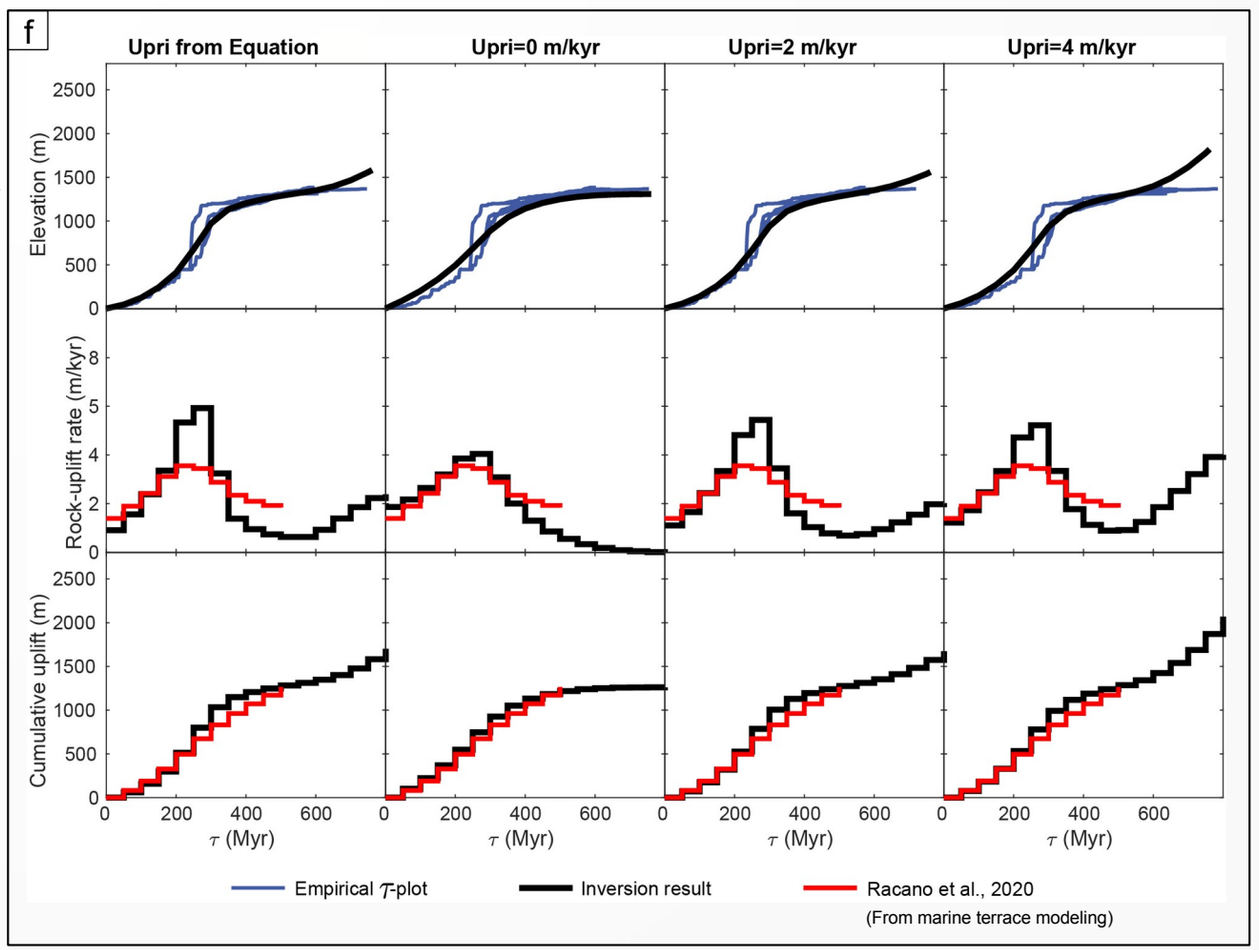

a) Study area of Racano et al., 2021; b) Inversions for catchments 1, 2, 3, 4; c) Inversions for catchments 5, 6, 7, 8; d) average rock-uplift trend for the western side of the study area (catchments from1 to 4); d) average rock-uplift trend for the western side of the study area (catchments from5 to 8); f) river inversion results varying U_{prior} for catchment 5.

Fixing U^*_{pri}

Racano et al., 2021

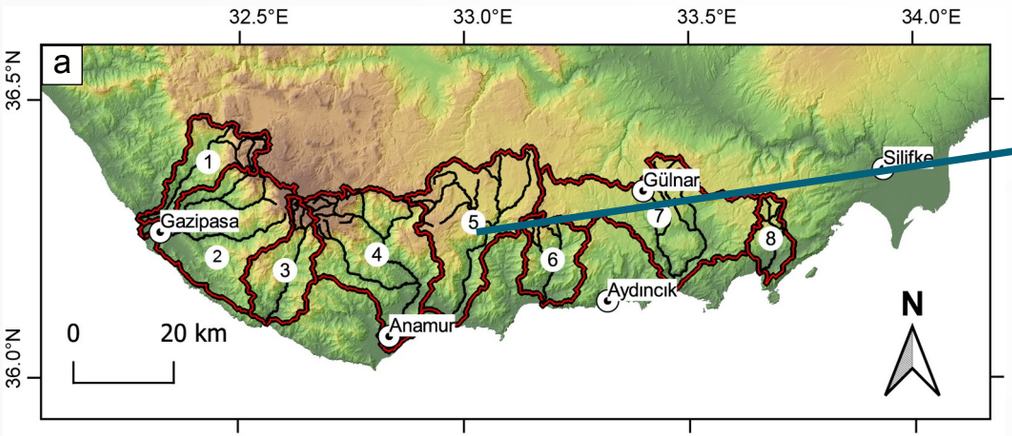

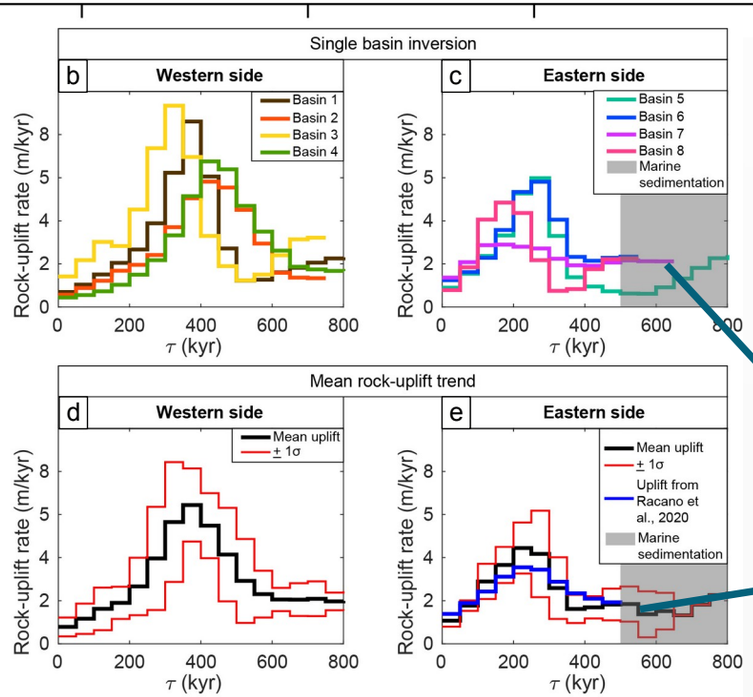

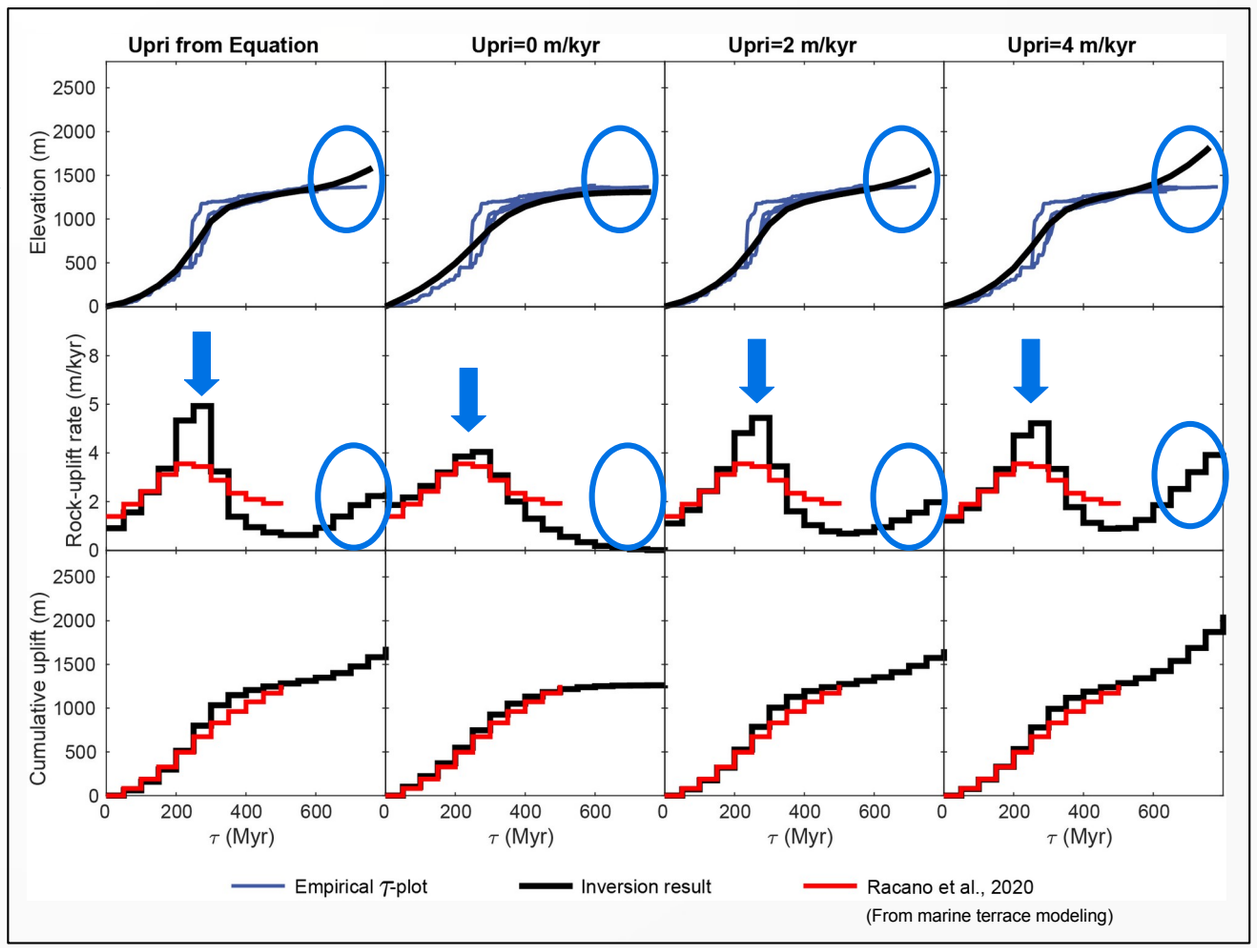

Equation 12 overestimate the uplift for the older stages of river histories

Fixing U^*_{pri}

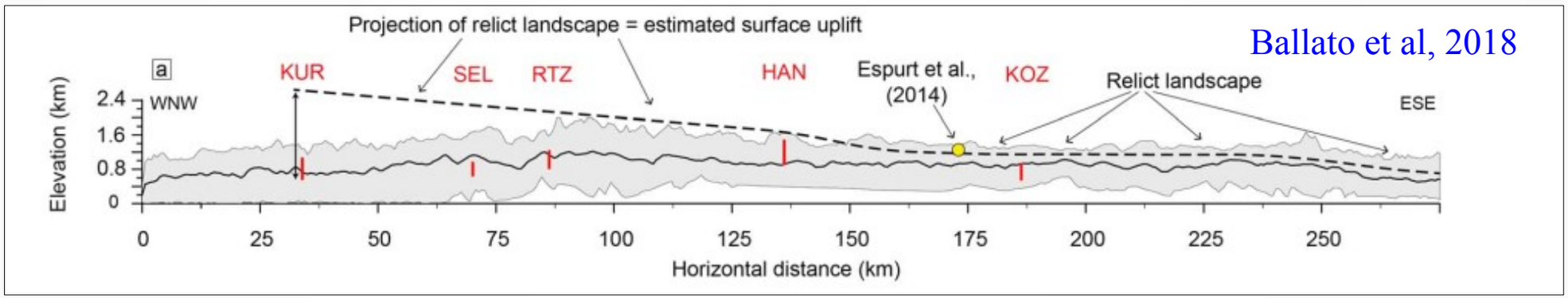

$$for\ A_0 = 1 \qquad U^* = k_{sn} = \left(\frac{U}{K}\right)^{\frac{1}{n}}$$

We propose a different way to estimate U^*_{pri} in a non-dimensional river linear inversion. Imposing A_0=1 (and for n=1), we show that $\boldsymbol{U^*}$ is equivalent to the channel steepness index (k_{sn}). We next considered that Ballato et al. (2018) identified a relict landscape located above an average elevation of 1000 m.a.s.l. in the Sinop Range. In our inversion approach, the U^*_{pri} used is the mean k_{sn} ($\pm 1\sigma$), for each analyzed catchment upstream of the elevation limit of this paleolandscape. In this way, our U^*_{pri} should represent the average rock-uplift rate before the uplift of the relict surface. We refer to the elevation range from which the average k_{sn} is estimated as z_{prior}. For catchments that do not reach the elevation of the paleolandscape, we arbitrary set z_{prior} to the first 150 m of elevation from the channel-head of river profiles.

Testing U^*_{pri} and χ-steps for the inversion

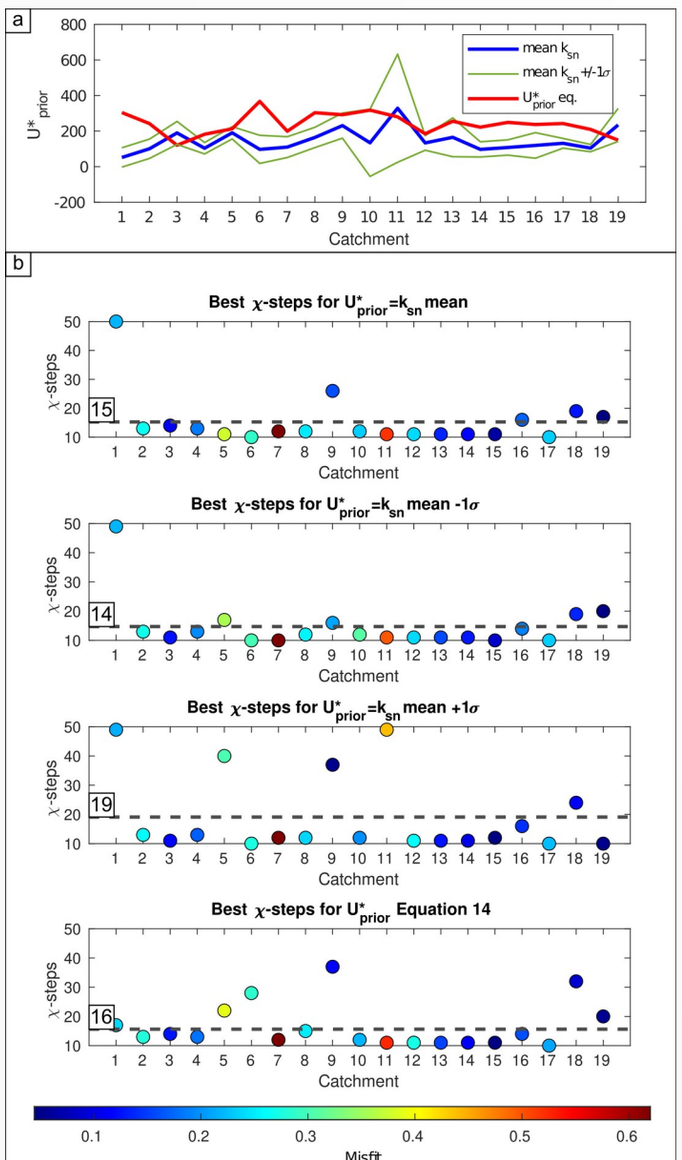

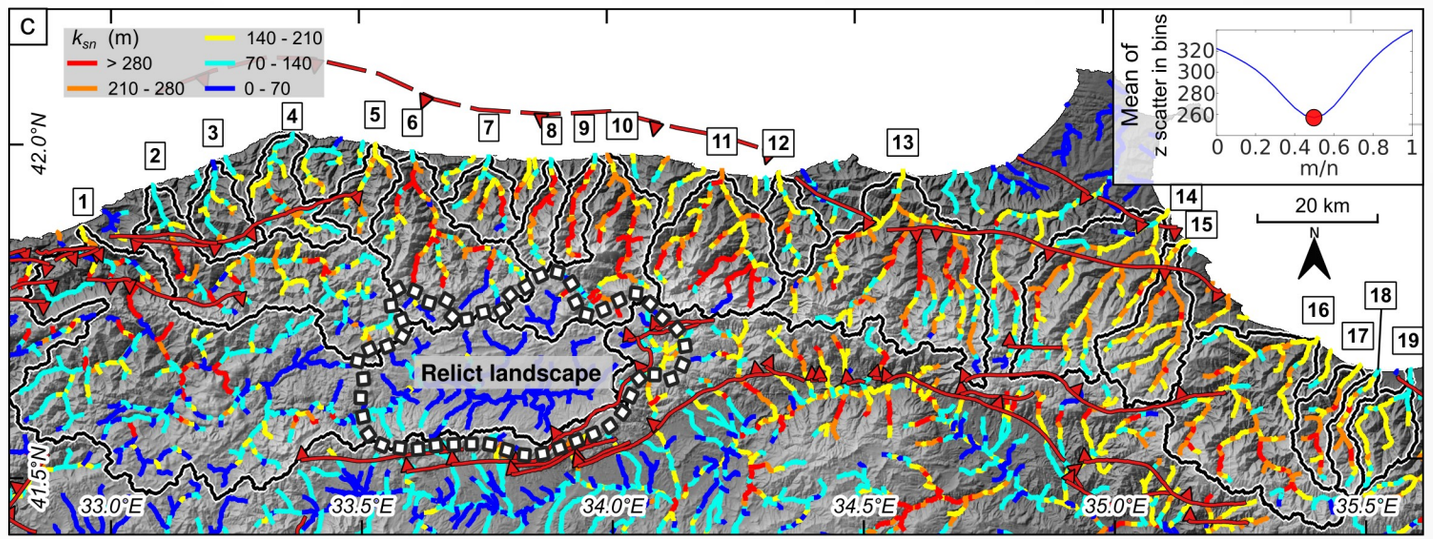

(a) Difference between U^*_{prior} estimated from Equation 12 and U^*_{prior} $\pm 1\sigma$ from the average k_{sn} above z_{prior};

(b) estimation of the best χ-steps for the river inversion;

(c) k_{sn} map of the Sinop Range, estimation of the best fit m/n by the χ-z plot minimization method from Goren et al., 2014, inverted catchments (see next pages) and location of the relict landscape.

$$Misfit = \frac{1}{N-q}\sqrt{\sum_{i=1}^{N}\left(z_i - z_{mod}\right)^2}$$ Parker, 1994

Testing U^*_{pri} and χ-steps for the inversion

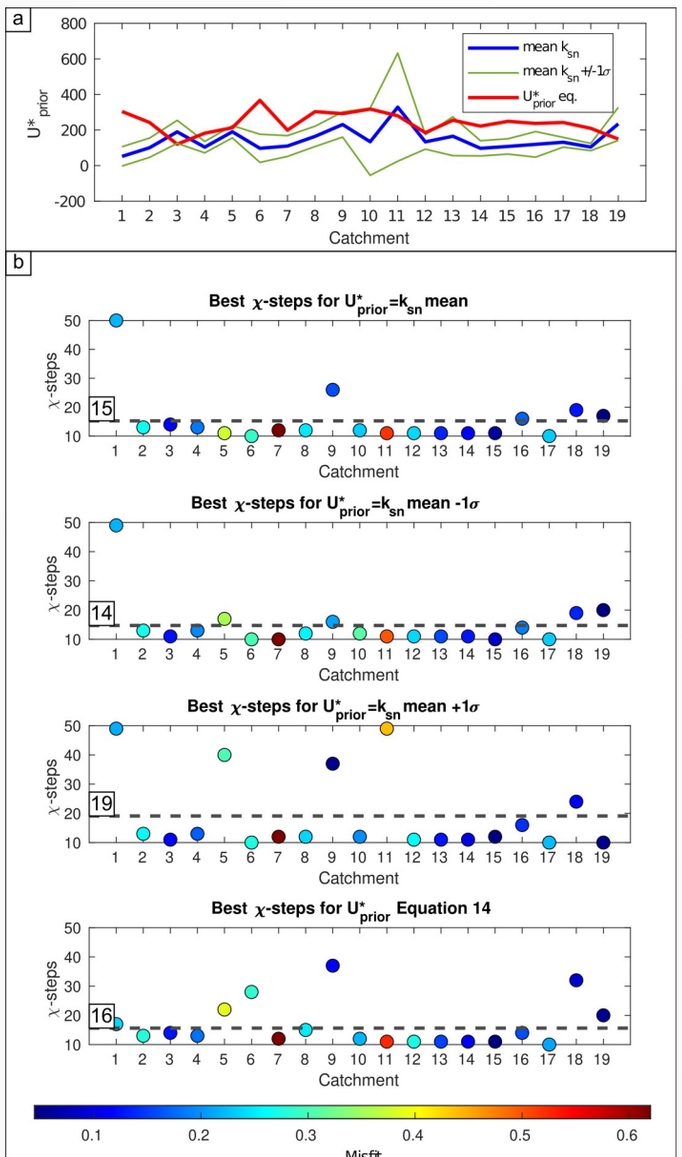

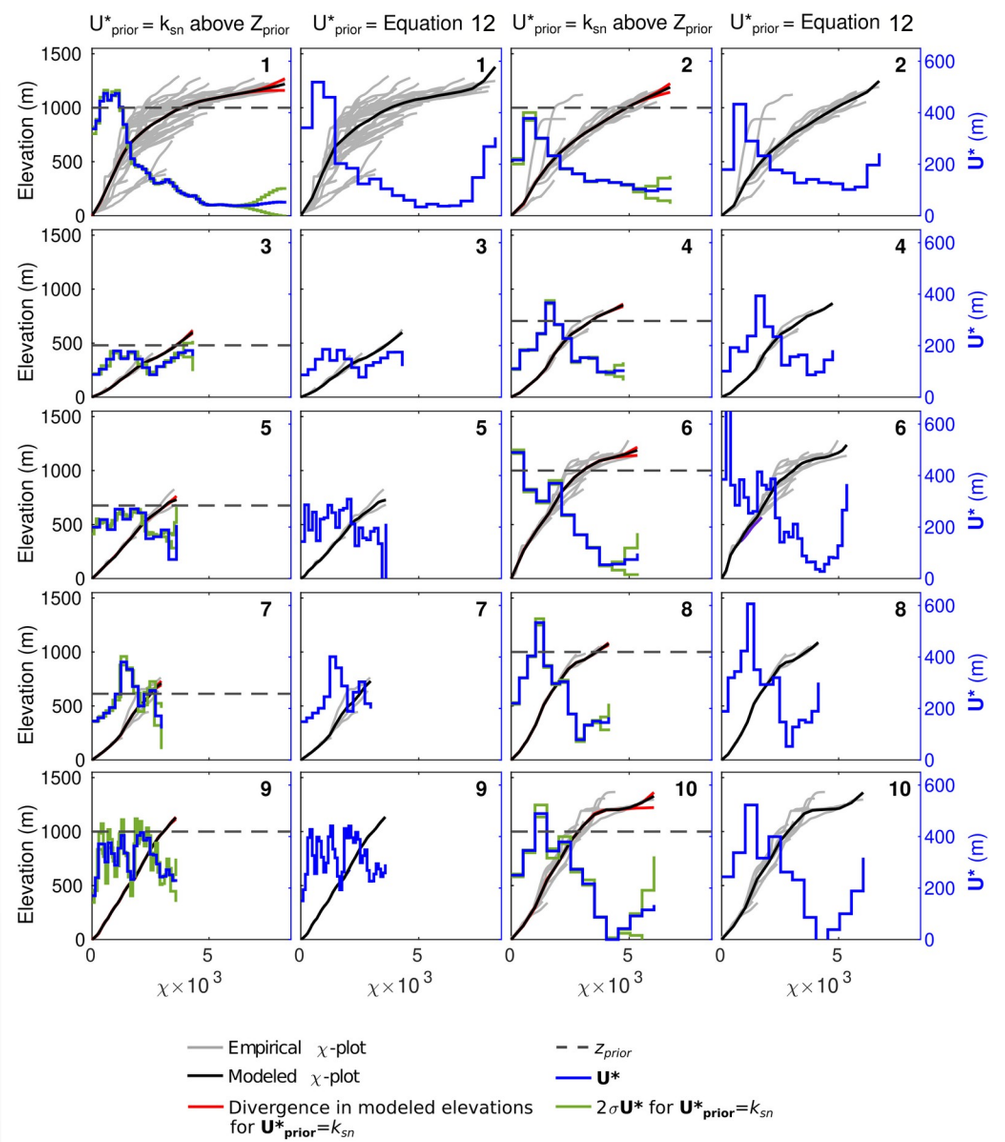

Testing U^*_{pri} and χ-steps for the inversion

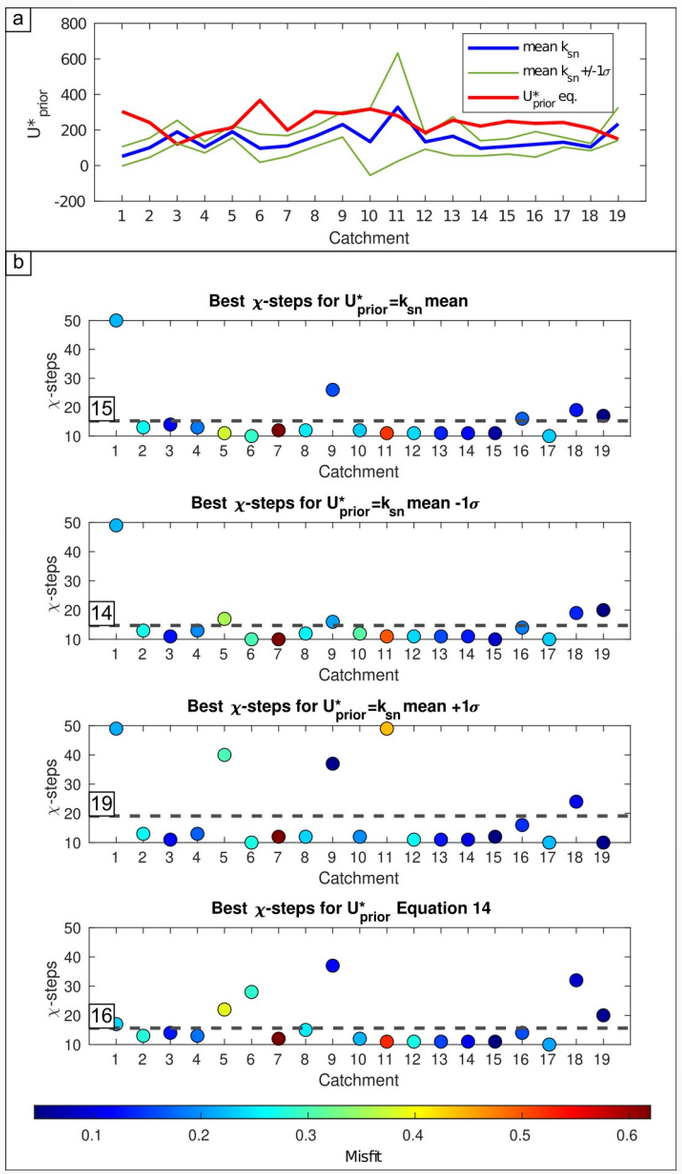

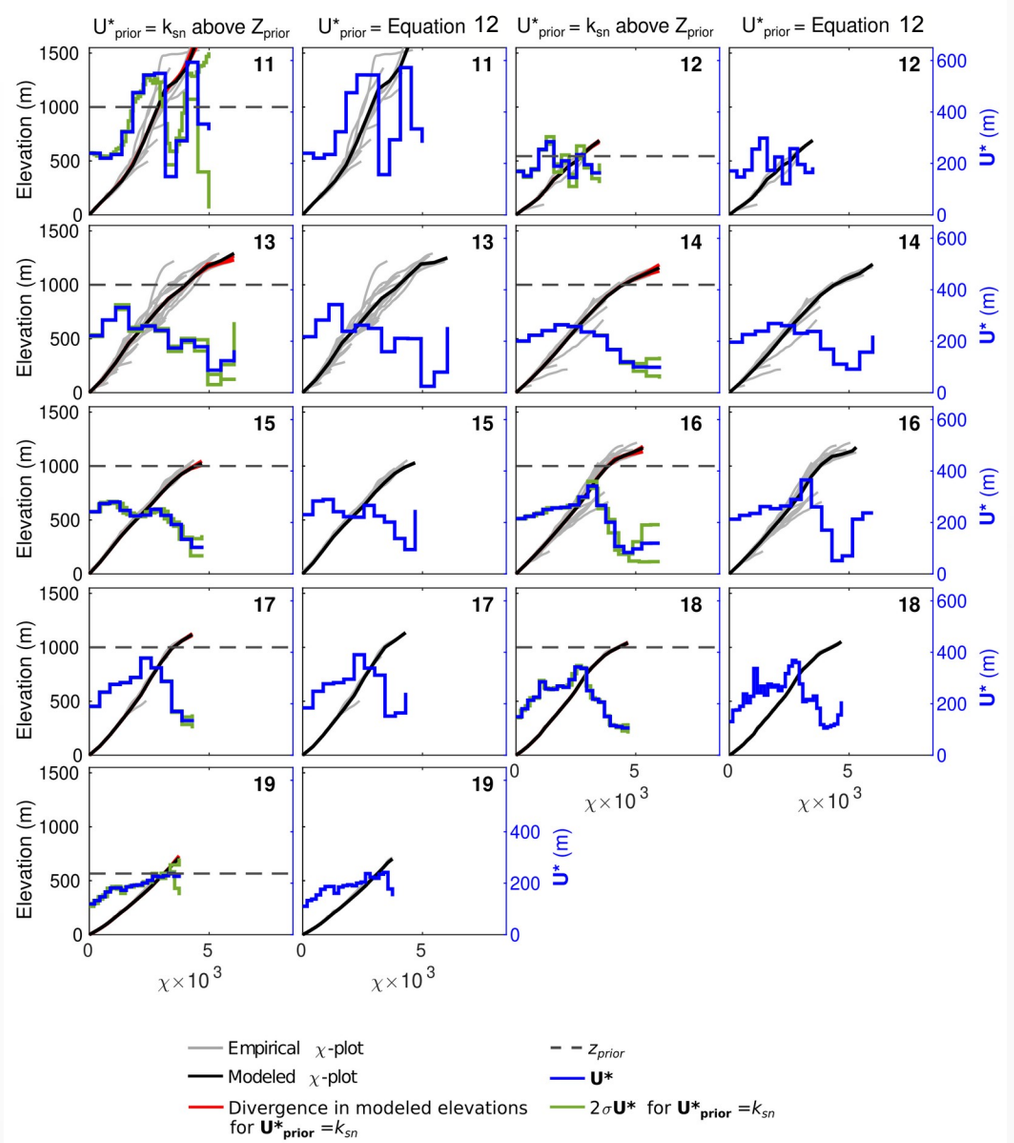

River linear inversion

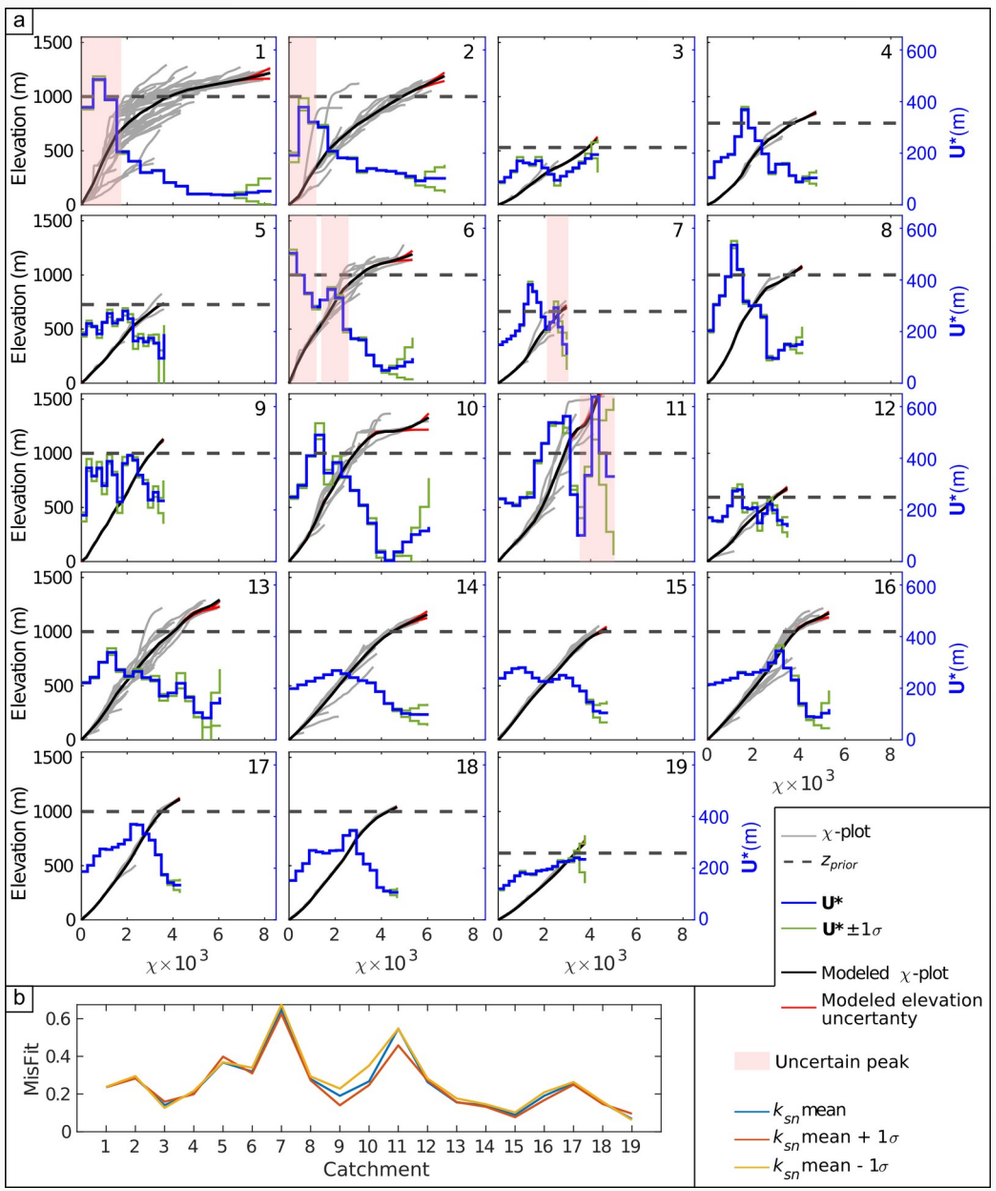

FINAL SET UP

$m/n = 0.5$

$A_0 = 1$

U^*_{prior} = average k_{sn} $\pm 1\sigma$ above z_{prior}

X-steps = 16 (average of the inversions made for U^*_{prior} $k_{sn} \pm 1\sigma$)

a) Linear inversion results fro the 19 selected catchments;

b) Inversion misfit;

River linear inversion

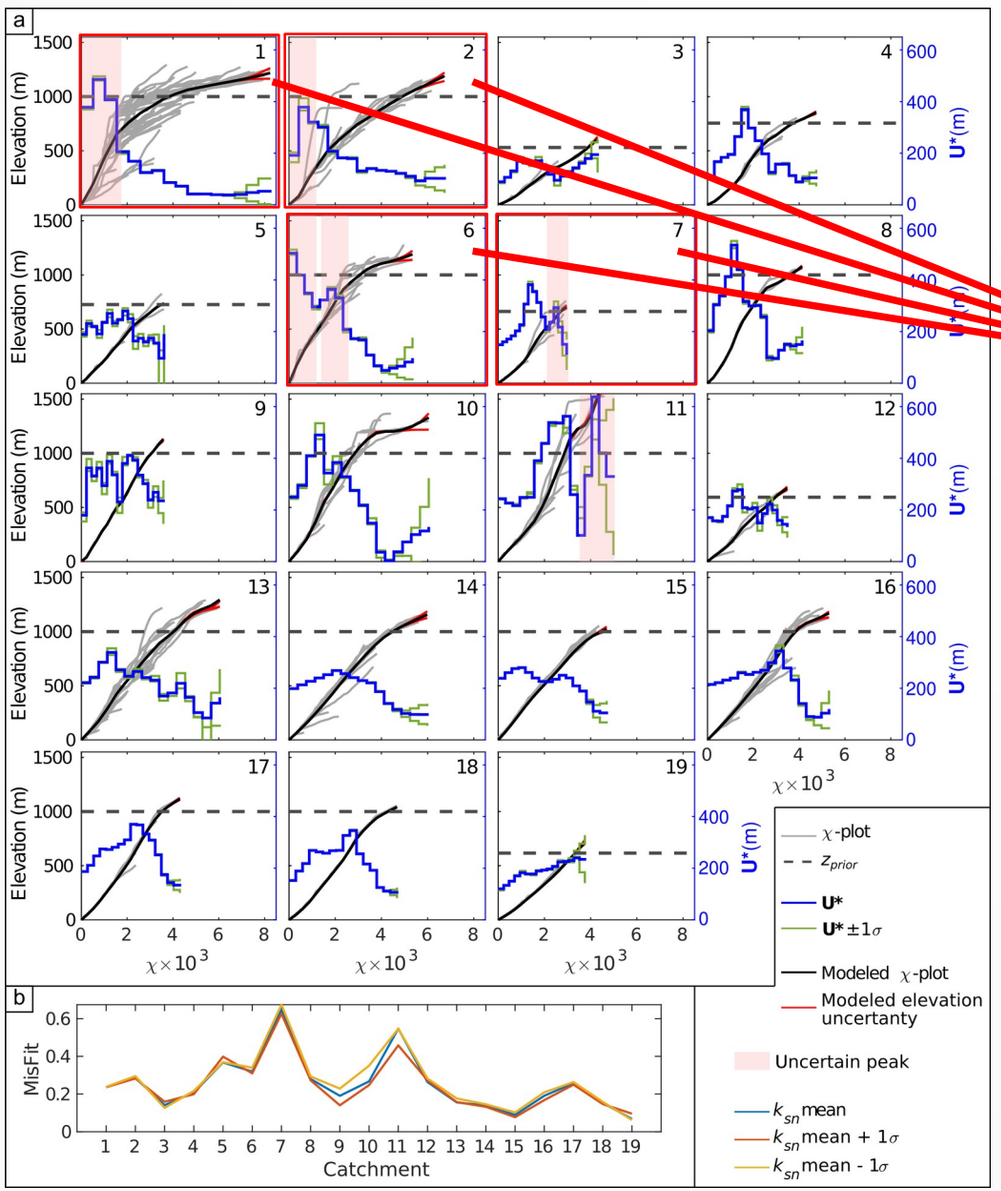

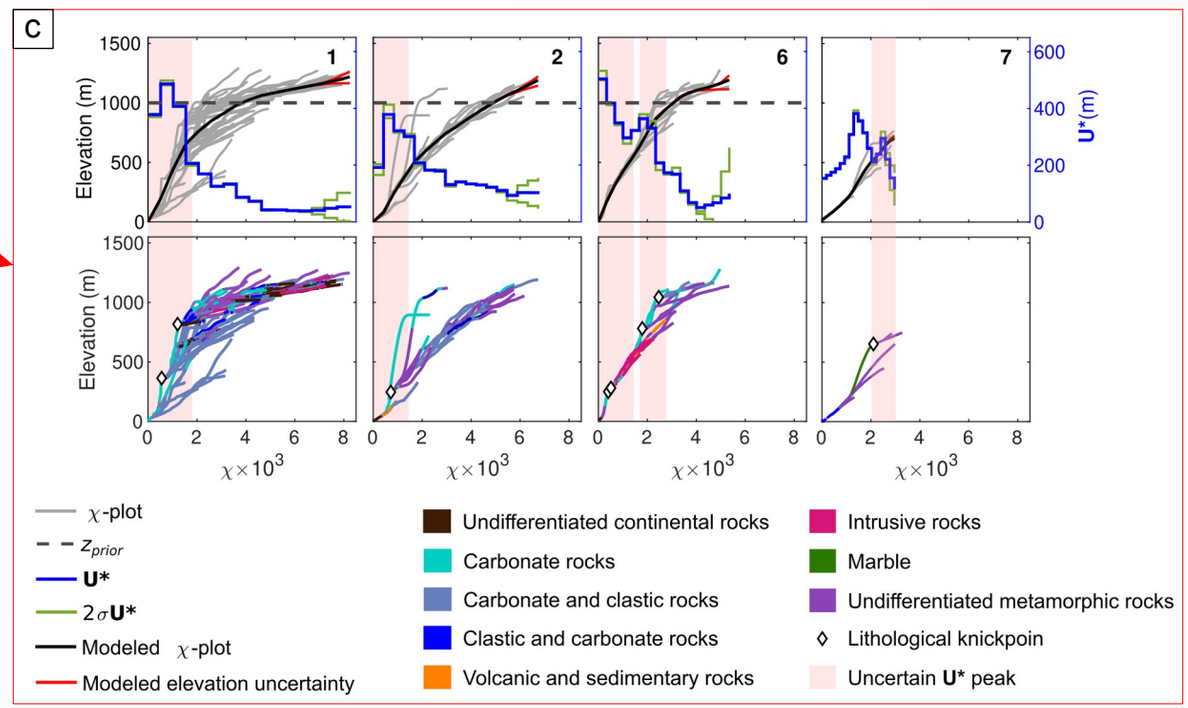

a) Linear inversion results fro the 19 selected catchments;

b) Inversion misfit;

c) Effects of static knickpoints on river linear inversions.

River linear inversion

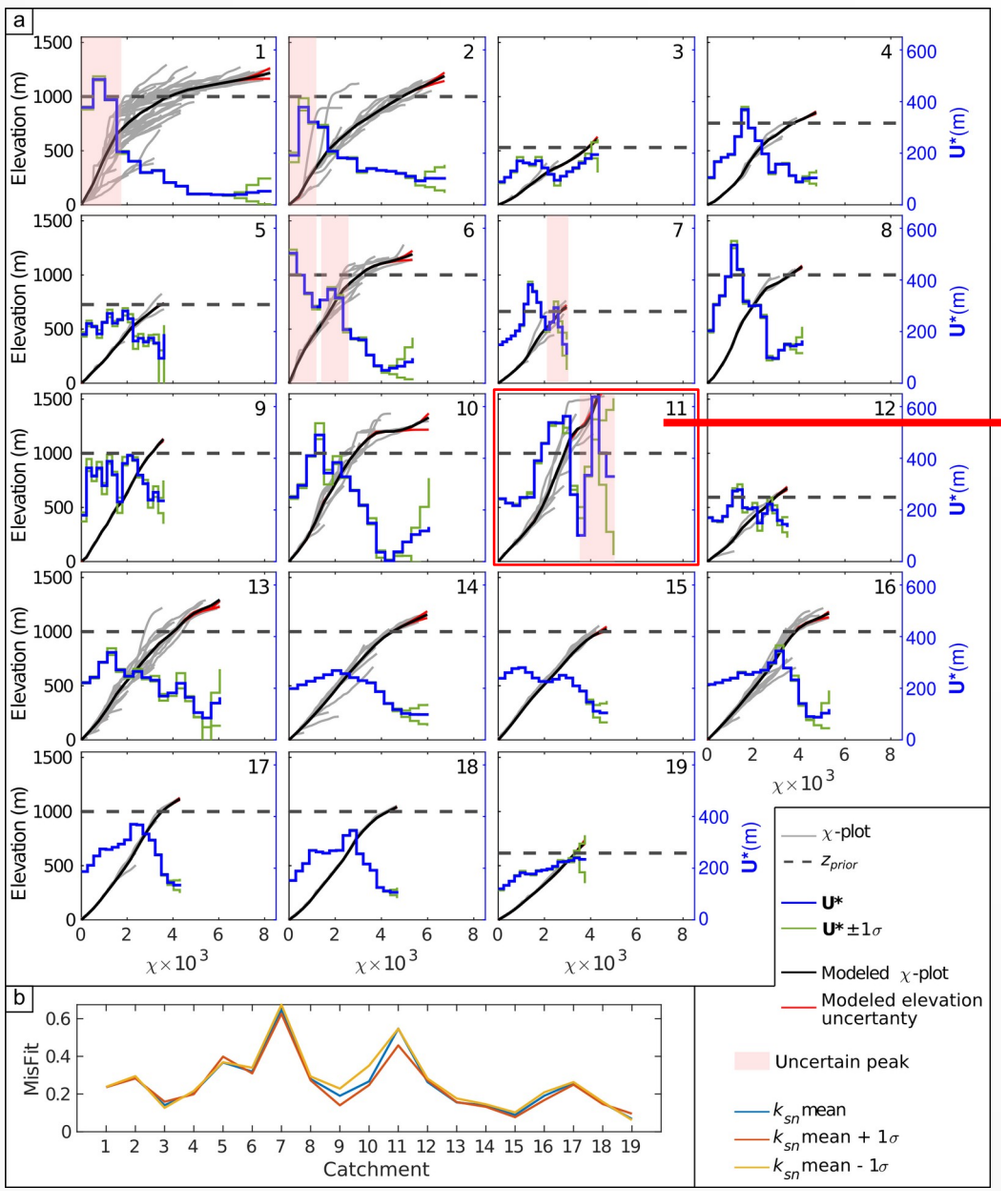

Giachetta & Willet, 2018

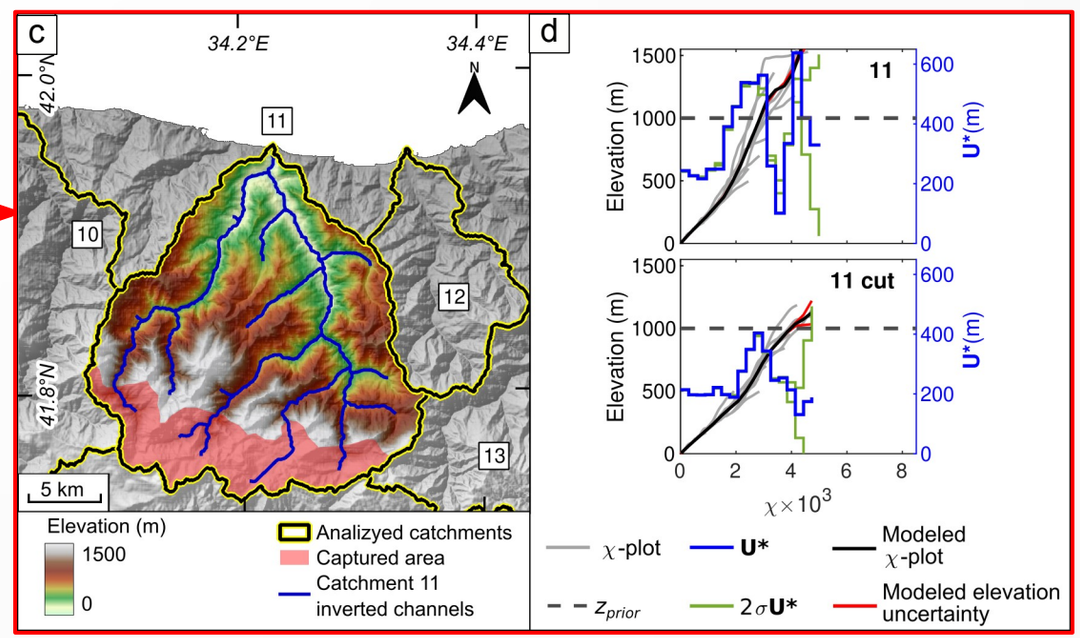

a) Linear inversion results fro the 19 selected catchments;

b) Inversion misfit;

c) Supposed recent capture area;

d) River inversion with and removing the supposed captured area.

Steepness index, denudation rates and erosion parameter

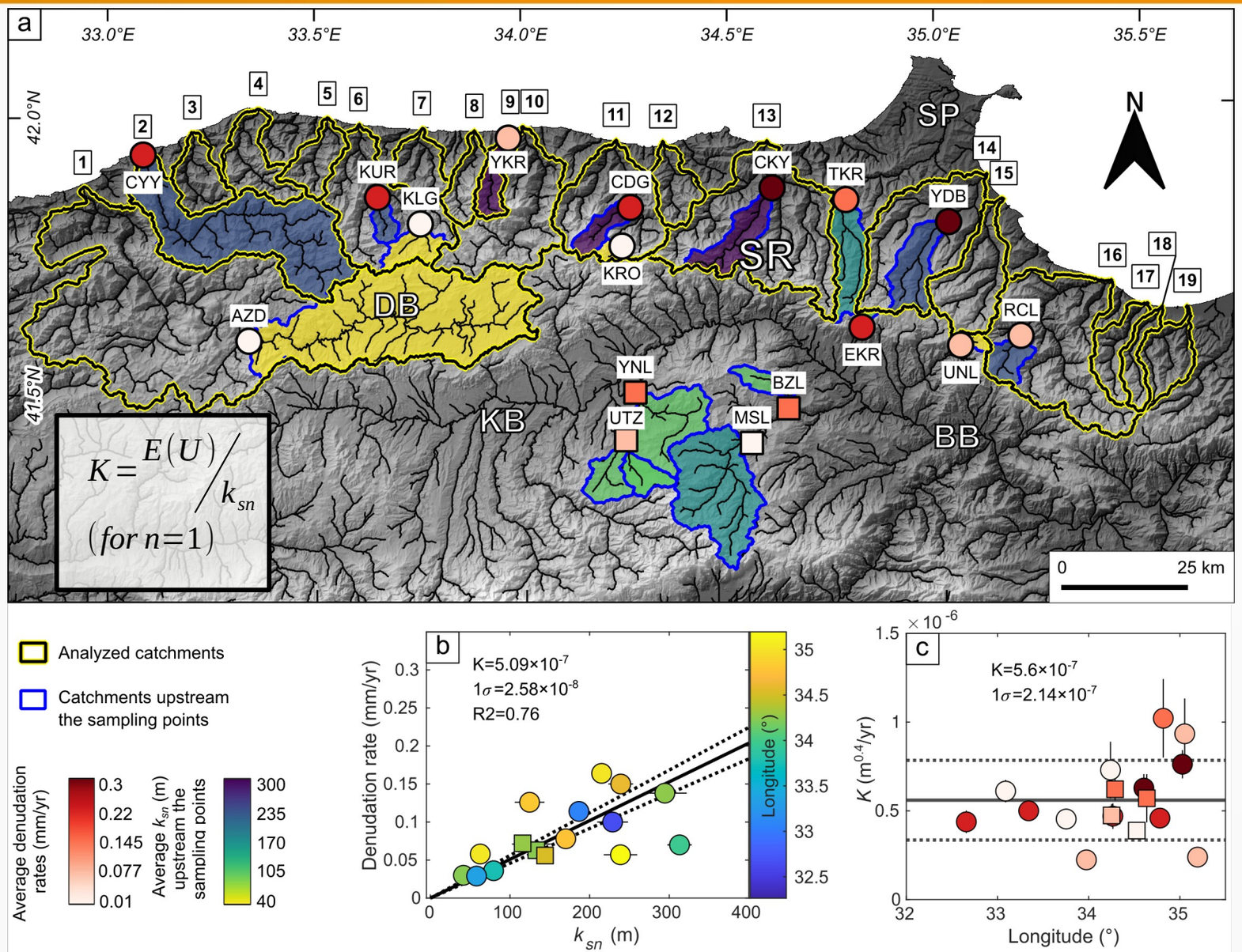

a) Sampling point location for cosmogenic wide denudation rates and average k_{sn} above the sampling points;

b) erosion parameter (K) estimation from linear fit of k_{sn} vs denudation rate plot;

(c) estimation of the erosion parameter (K) by dividing for each sampling location the denudation rate by the associated k_{sn}.

River linear inversion

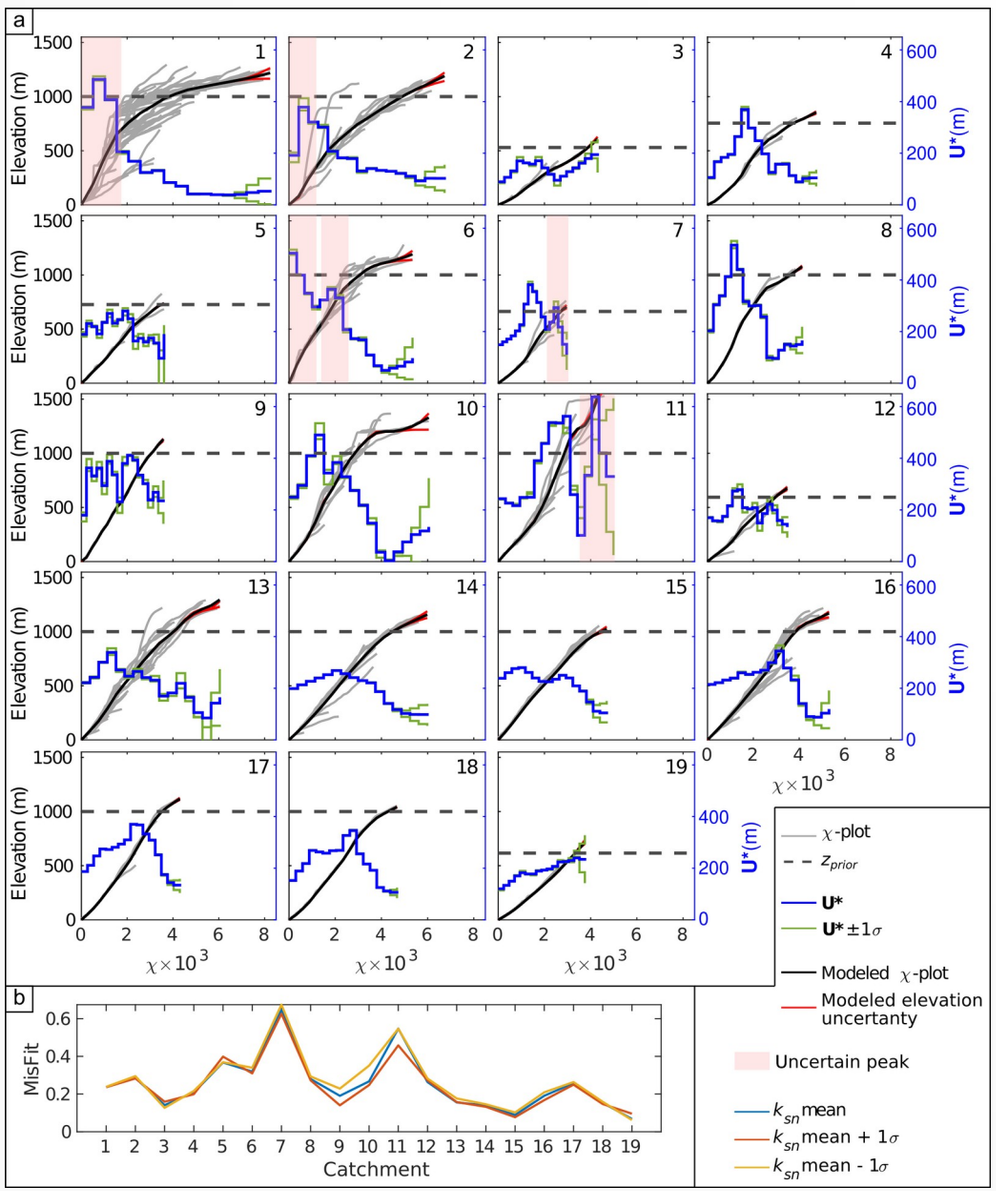

$$\tau = \frac{\chi}{K A_0^m} \qquad U = U^* \times K A_0^m$$

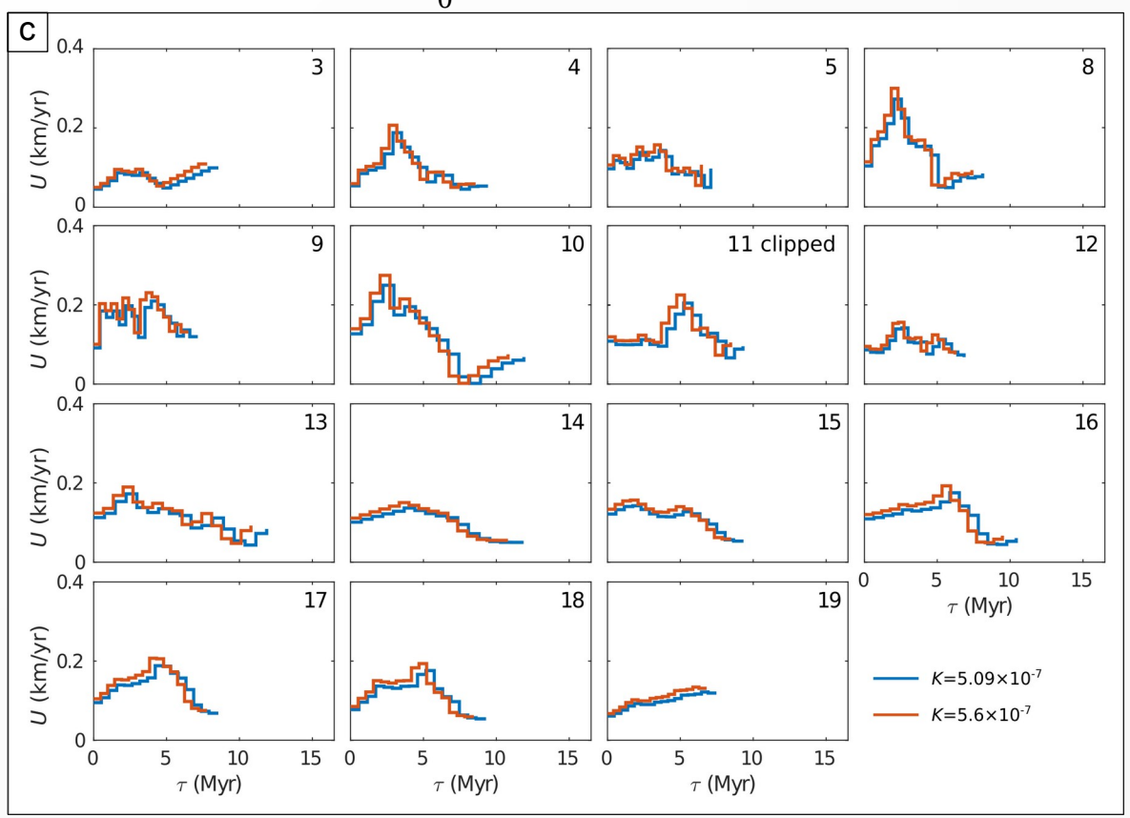

a) Linear inversion results fro the 19 selected catchments;

b) Inversion misfit;

c) Rock-uplift (U) variation through time (τ) by scaling χ and **U*** for the K values estimated by the linear fit of k_{sn} vs denudation rates (blue line), and from the average of the K values estimated by dividing the denudation rates by the associated k_{sn} in the sampling locations (orange line).

Rock-uplift history of the Sinop Range

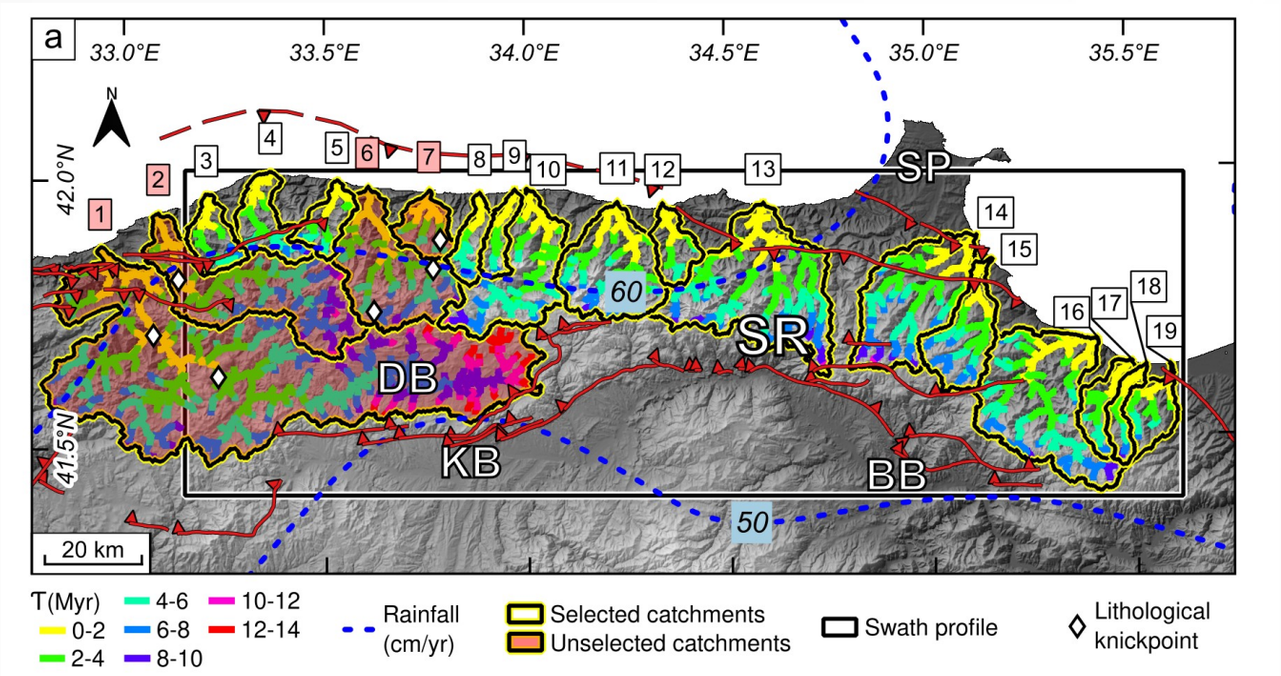

a) τ map of the inverted catchments, trace of the swath profile (b) and excluded catchments with static knickpoints (red);

b) swath profile of the Sinop Range and location of the relict landscape and of the catchments selected to build the rock-uplift and uplift acceleration models (c and d);

c) Rock-uplift model of the Sinop Range;

d) Uplift acceleration model of the Sinop Range and direction of the uplift migration.

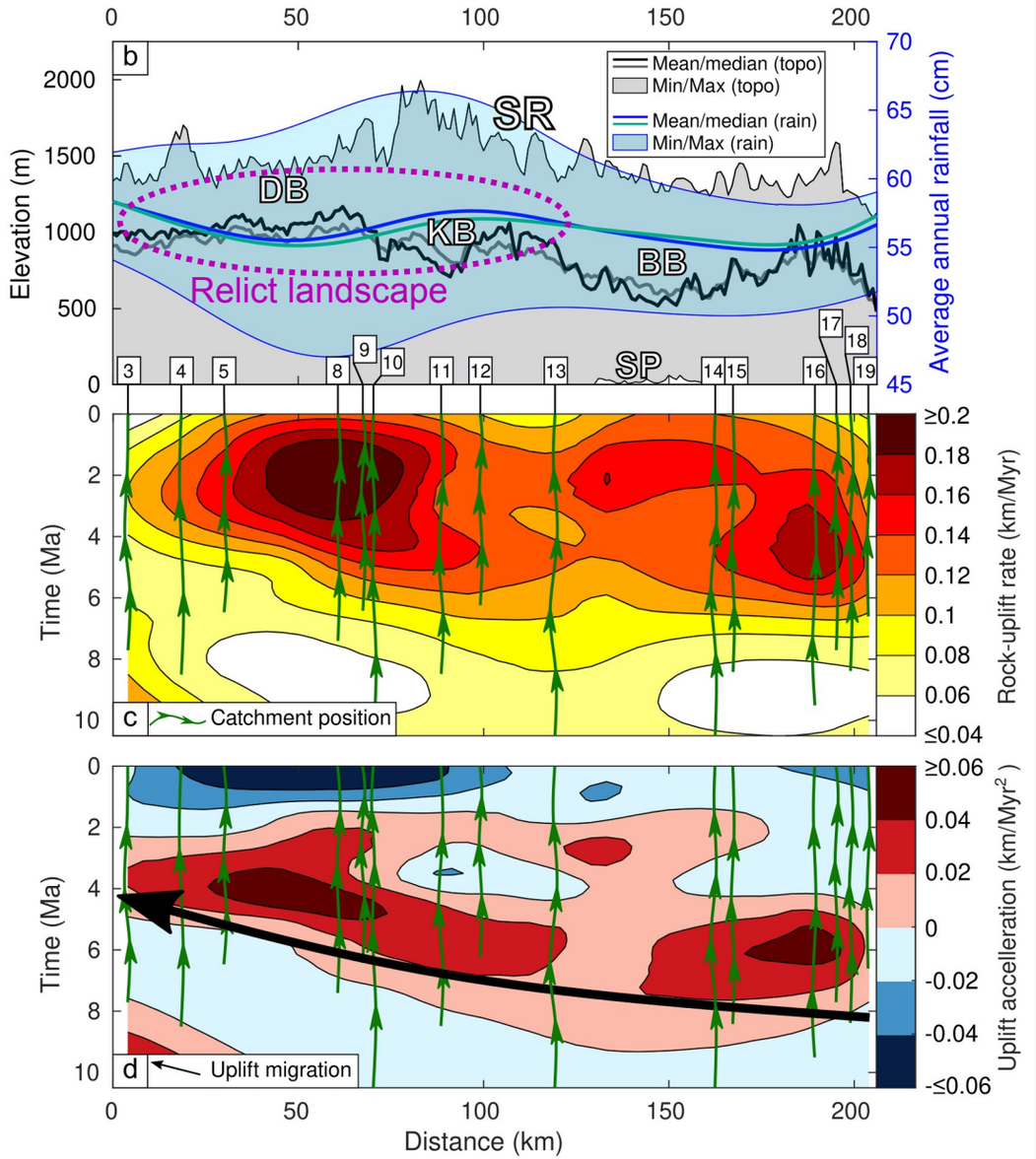

Propagation of the North Anatolian Fault

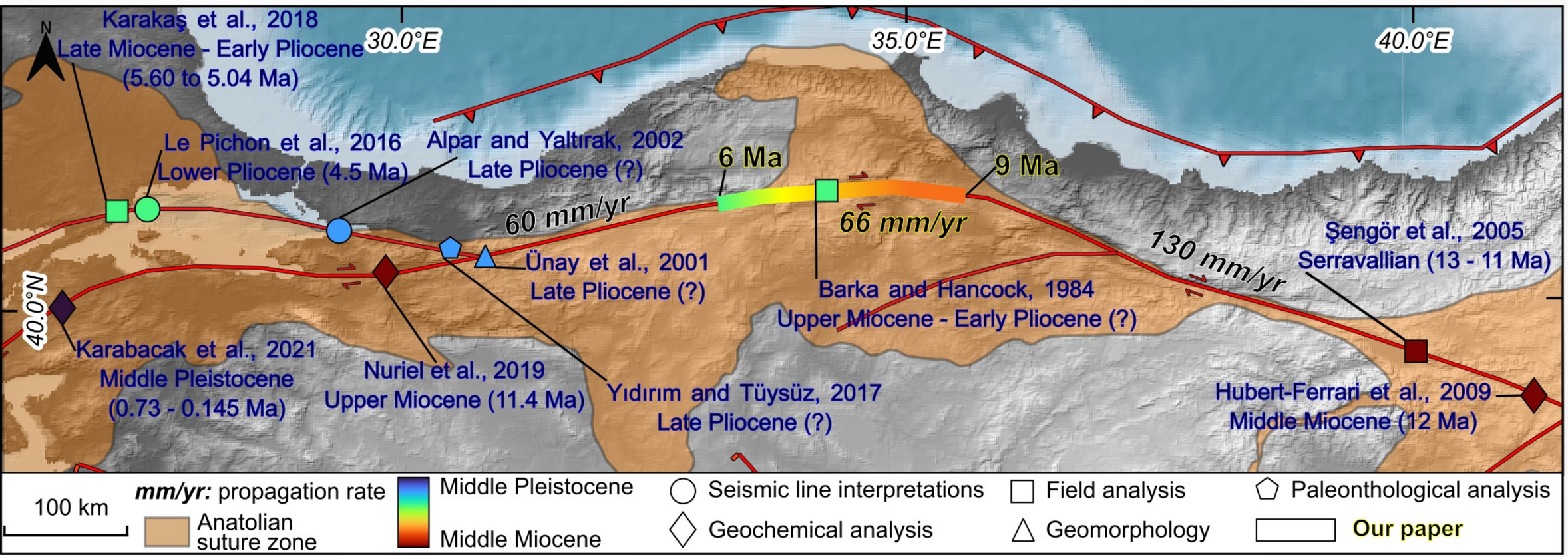

Age of the faulting onset of the North Anatolian Fault from several published papers classified by analysis type and inferred propagation rates

References:

- Alpar, B., & Yaltırak, C. (2002). Characteristic features of the North Anatolian Fault in the eastern Marmara region and its tectonic evolution. Marine Geology, 190(1–2), 329–350.
- Ballato, P., Uba, C. E., Landgraf, A., Strecker, M. R., Sudo, M., Stockli, D. F., et al. (2011). Arabia-Eurasia continental collision: Insights from late Tertiary foreland-basin evolution in the Alborz Mountains, northern Iran. Bulletin of the Geological Society of America, 123(1–2), 106–131.
- Barka, A. A., & Hancock, P. L. (1984). Neotectonic deformation patterns in the convex-northwards arc of the North Anatolian fault zone. Geological Society, London, Special Publications, 17(1), 763–774.
- Gallen, S. F. (2018). Lithologic controls on landscape dynamics and aquatic species evolution in post-orogenic mountains. Earth and Planetary Science Letters, 493, 150–160.
- Giachetta, E., & Willett, S. D. (2018). Effects of River Capture and Sediment Flux on the Evolution of Plateaus: Insights From Numerical Modeling and River Profile Analysis in the Upper Blue Nile Catchment. Journal of Geophysical Research: Earth Surface, 123(6), 1187–1217.
- Goren, L., Fox, M., & Willett, S. D. (2014). Tectonics from fluvial topography using formal linear inversion: Theory and applications to the Inyo Mountains, California. Journal of Geophysical Research: Earth Surface, 119(8), 1651–1681.
- Howard, A. D., & Kerby, G. (1983). Channel changes in badlands. GSA Bulletin, 94(6), 739–752.
- Hubert-Ferrari, A., King, G., Woerd, J. van der, Villa, I., Altunel, E., & Armijo, R. (2009). Long-term evolution of the North Anatolian Fault: new constraints from its eastern termination. Geological Society, London, Special Publications, 311(1), 133–154.
- Karabacak, V., Sançar, T., Yildirim, G., & Uysal, I. T. (2022). When did the North Anatolian fault reach southern Marmara, Turkey? Geology, 50(4), 432–436.
- Karakaş, Ç., Armijo, R., Lacassin, R., Suc, J.-P., & Melinte-Dobrinescu, M. C. (2018). Crustal Strain in the Marmara Pull-Apart Region Associated With the Propagation Process of the North Anatolian Fault. Tectonics, 37(5), 1507–1523.
- Le Pichon, X., Şengör, A. M. C., Kende, J., İmren, C., Henry, P., Grall, C., & Karabulut, H. (2016). Propagation of a strike-slip plate boundary within an extensional environment: the westward propagation of the North Anatolian Fault. Canadian Journal of Earth Sciences, 53(11), 1416–1439.
- Nuriel, P., Craddock, J., Kylander-Clark, A. R. C., Uysal, I. T., Karabacak, V., Dirik, R. K., et al. (2019). Reactivation history of the North Anatolian fault zone based on calcite age-strain analyses. Geology, 47(5), 465–469.
- Parker, R. L. (1994), Geophysical Inverse Theory, Princeton Univ. Press, Princeton, N. J.
- Perron, J. T., & Royden, L. (2013). An integral approach to bedrock river profile analysis: Integral approach to river profile analysis. Earth Surface Processes and Landforms, 38(6), 570–576.
- Racano, S., Schildgen, T. F., Cosentino, D., & Miller, S. R. (2021). Temporal and spatial variations in rock uplift from river-profile inversions at the Central Anatolian Plateau southern margin. Journal of Geophysical Research: Earth Surface, 126, e2020JF006027.
- Şengör, A. M. C., Tüysüz, O., İmren, C., Sakınç, M., Eyidoğan, H., Görür, N., et al. (2005). THE NORTH ANATOLIAN FAULT: A NEW LOOK. Annual Review of Earth and Planetary Sciences, 33(1), 37–112.
- Tarantola, A. (1988). Inverse problem theory. Methods for data fitting and model parameter estimation. Geophysical Journal International, 94(1), 167–168.
- Ünay, E., Emre, Ö., Erkal, T., & Keçer, M. (2001). The rodent fauna from the Adapazarı pull-apart basin (NW Anatolia): its bearings on the age of the North Anatolian fault. Geodinamica Acta, 14(1–3), 169–175.
- Whipple, K. X., & Tucker, G. E. (1999). Dynamics of the stream-power river incision model: Implications for height limits of mountain ranges, landscape response timescales, and research needs. Journal of Geophysical Research, 104(B8), 17661–17674.
- Yıldırım, C., & Tüysüz, O. (2017). Estimation of the long-term slip, surface uplift and block rotation along the northern strand of the North Anatolian Fault Zone: Inferences from geomorphology of the Almacık Block. Geomorphology, 297, 55–68.